PNC-TN9410 88-091

FULL SCALE DRYOUT TEST IN DOWNWARD FLOW ON AN ATR 36-ROD BUNDLE

August, 1988

OARAI ENGINEERING CENTER

POWER REACTOR AND NUCLEAR FUEL DEVELOPMENT CORPORATION

複製又はこの資料の入手については，下記にお問い合わせください。
〒311-13　茨城県東茨城郡大洗町成田町4002
動力炉・核燃料開発事業団
大洗工学センター　システム開発推進部・技術管理室

Enquires about copyright and reproduction should be addressed to: Technology Management Section O-arai Engineering Center, Power Reactor and Nuclear Fuel Development Corporation 4002 Narita-cho, O-arai-machi, Higashi-Ibaraki, Ibaraki-ken, 311-13, Japan

動力炉・核燃料開発事業団（Power Reactor and Nuclear Fuel Development Corporation）

PNC-TN9410 88-091
August. 1988

FULL SCALE DRYOUT TEST IN DOWNWARD FLOW ON AN ATR 36-ROD BUNDLE*

Takaaki Sakai** and Satoru Sugawara**

Power Reactor and Nuclear Fuel Development Corporation
4002 Narita, Oarai-machi, Ibaraki-ken, 311-13, Japan

ABSTRACT

Dryout power in downward flow has been measured on an electrically heated full-scale mock-up of a 36-rod bundle, which is designed for the demonstration plant of the Advanced Thermal Reactor(ATR) developed in Japan. Dryout power data obtained from the present tests were compared with experimental data in upward flow, and were used for developing a correlation of the dryout power vs. mass velocity. From the present study, it is concluded that the dryout power in downward flow depends on mass velocity in more complicated manner than in upward flow, especially in low mass velocity, where the dryout power reduced to 25% of the value in upward flow.

---

* To be presented to "The third international topical meeting on nuclear power plant thermal hydraulics and operations", November 14-17, 1988, Sheraton Walker Hill, Seoul, Korea.

** Reactor Engineering Section, Safety Engineering Division, O-arai Engineering Center, PNC

CONTENTS

1. INTRODUCTION

The Advanced Thermal Reactor(ATR) developed in Japan is a heavy-water-moderated light-water-cooled pressure-tube-type reactor. In the event of the flow reversal in a pressure tube under a postulated accidental condition of the ATR, a fuel bundle is would be cooled with steam-water two-phase downward flow. Therefore, The coolability of the downward flow is a primary concern in thermal-hydraulic design and safety evaluation of the ATR.

So far several experiments have been conducted to find out dryout characteristics in downward flow, and unfavorably show that coolability would be markedly reduced in downward flow, compared with that in upward flow. For example, Cumo et al.[1] found out that dryout power decreases by 35% in downward flow of freon compared with that in upward flow. Mishima et al.[2] measured critical heat flux at the low velocity and low pressure condition, and concluded that the decrease in critical heat flux in downward flow is due to bubble stagnation. Moreover, Collier[3] suggested that the dryout power in the downward flow starts to decrease rapidly at the minimum flow velocity.

However, those results were not directly applied to thermal-hydraulic analysis of the ATR, having been obtained from tests which do not simulate an actual ATR bundle.

Consequently, full scale tests were performed in the 14MW Heat Transfer Loop (HTL) at Oarai Engineering Center of PNC, to investigate dryout power and other hydraulic characteristics of the ATR fuel bundle in downward flow.

2. EXPERIMENTS

2-1. Apparatus

The tests were conducted for a full scale mock-up of a fuel bundle to be used in the 600 MWe ATR demonstration plant. The mock-up consists of 36 heated tubes and 1 non-heated tube. These tubes are assembled in a heater bundle by top and bottom tie plates and 16 ring-type spacers. As shown in Fig.1, the heated tubes, simulating fuel rods, form in three concentric circular layers, surrounding the non-heated center tube. The heated tubes are 14.5 mm in outer diameter, and made from stainless steel; the non-heated center tube has the same outer diameter. As a result of this tube configuration, the heater bundle has the following thermal-hydraulic features a heated length of 3.7m, a heat transfer area of 6.06m^2, a flow area of 4,788mm^2, and a hydraulic equivalent diameter of 9.3mm.

Electric DC current is supplied to the heated tubes; the heat is generated by the Joule effect due to electric resistance inherent in the heated tubes. The heated tubes are axially non-uniform in wall thickness to provide a shaped axial cosine power distribution with a peak-to-average power ratio of 1.3. The average wall thickness of the heated tubes in each layer is adjusted to provide the radial power distribution of 1.2/0.84/0.7 from the outer to inner layer. Chromel-Alumel(C-A) thermocouples of 0.5mm outer diameter for the detection of dryout are soldered with silver on the surface of the heated tubes. Thermocouples are located 10mm upstream and downstream of the spacers, as shown in Fig.1.

The bundle was housed in a simulated pressure tube made from Al_2O_3, and assembled into a test section together with electrodes and a high pressure container. A cross sectional view of the test section is given in Fig.2. As seen in Fig.3, the test section was built into the HTL with a piping layout such that downward flow could develop in the pressure tube. The

coolant condition at the inlet of test section was fixed with a pre-heater. The inlet flow rate was measured with a turbine flow meter installed immediately downstream of a recirculation pump. System pressure was fixed by adjusting the cooling capacity of a high pressure condenser.

2-2. Test condition

The tests were carried out under the following conditions:

Pressure	:	7.0	MPa
Mass velocity	:	0 - 2,800	kg/m^2s
Heat power	:	0 - 9.0	MW
Inlet temperature	:	548	K

These conditions were determined on the basis of normal ATR operating conditions which are: a pressure of 7.0 MPa, a mass flux of 2,100 kg/m^2s, an average heating power per fuel bundle of 2.98 MW, and an inlet temperature of 548 K. Measuring accuracies were estimated at $\pm$0.5K for inlet temperature, $\pm$0.5% for system pressure, $\pm$3% for inlet flow rate, and $\pm$1% for electric power supplied to the heater bundle.

After coolant conditions at the inlet of the test section were fully fixed, the power of the heater bundle was increased so gradually that steady state condition could be kept. An onset of dryout was recognized by a rapid rise in temperature of the heated tube surfaces.

3. RESULTS AND DISCUSSION

3-1. Dryout power in downward flow

Dryout power data obtained from the present tests are plotted in Fig.4 against the mass velocity, together with dryout data for upward flow. At high mass velocity, dryout power is precisely equal for downward and upward flows. In contrast to this, dryout power is much smaller in downward flow than in upward flow at low mass velocities of about 725 kg/m^2s or less. In order to show this situation more clearly, the ratio of dryout power between the downward and upward flows are indicated in Fig.5. This figure clearly suggests that thermal-hydraulic features in downward flow can be separated into three phases in terms of the dependence of the dryout power ratio on mass velocity.

The first phase appears at mass velocities higher than 725 kg/m^2s. In this region, the ratio of dryout power between the upward and downward flows is independent of mass velocity and equal to unity, which presumes that the downward flow in the pressure tube equals the upward flow in terms of flow regime. That is, void and liquid in the two phase mixture would move together in the same direction, and the buoyancy effect could be considered negligible.

The second phase is recognized between 725 and 458 kg/m^2s. In this region, the dryout power ratio starts to decrease rapidly with decreasing of the mass velocity, and ultimately reaches a minimum at 458 kg/m^2s. The minimum dryout power is 75% smaller in downward flow than in upward flow. Buoyancy force generally prevents steam voids from moving downward. This buoyancy effect is enhanced as mass velocity decreases, and steam voids start to stay in the pressure tube for relatively longer time periods. Thus, void fraction in the pressure tube increases with decreasing mass velocity, which leads to deterioration of coolability of downward flow, and decreases the dryout power.

The third phase is observed at mass velocities smaller than 458 kg/m^{2}s. In this phase, the ratio of dryout power increases with decreasing mass velocity. The buoyancy force on steam voids exceeds drag force because the downward velocity of liquid is very small. The strength of the buoyancy force increases with decreasing mass velocity, and steam voids pass along the pressure tube over relatively shorter time periods. Thus, void fraction in the pressure tube decreases with decreasing mass flow velocity. This results in recovery of coolability of the downward flow.

The data for a 28-rod bundle is also indicated in Fig.5. There is no significant difference in the dependence of dryout power ratio on the mass velocity between the 36-rod and 28-rod bundles. This fact suggests that the dependence of the dryout-power ratio on the mass velocity is not affected by these bundle geometry.

The data of the present tests are compared in Fig.6 with Mishima's data measured at near atmospheric pressure in a rectangular duct. Figure 6 shows that the dryout power ratios obtained by Mishima depend upon the mass velocity in the same manner as the data of the present tests do. Hence, it can be concluded that the features in the dependence of the dryout power ratio on the mass velocity are not specific to the present experimental system. As mentioned previously, the dependence of the dryout-power ratio on the mass velocity can therefore be explained by the presumption that the downward flow changes its flow regime from counter-current to co-current with increasing mass velocity, whereas liquid and steam void always move co-currently in upward flow.

3-2. Dryout location

In order to examine the validity of the presumption given in the previous section, an attempt was made to find out how axial locations where dryout occurs change with increasing mass

velocity. As shown in Fig.7, the observed distribution of the locations strongly depends on mass velocity in downward flow, although dryout in upward flow always occurs near the top of the heated length. In downward flow with mass velocities higher than 580 kg/m^2s, dryout occurs at the exit in the same manner as upward flow. In the mass velocity region of downward flow lower than 580 kg/m^2s, the first dryout occurs in the middle or upper section of the pressure tube where the heat flux has the maximum value. This means that there is a flow regime transition from co-current downward flow to counter-current flow at a mass velocity of 580 kg/m^2s. When vapor flows downward together with liquid, void fraction is maximized at the lower exit of the pressure tube. Hence, the first dryout occurs near the lower exit in the same manner as with mass velocities higher than 580kg/m^2s. This supports the presumption that upward flow with mass velocities higher than 580kg/m^2s is co-current. On the other hand, void fraction relatively increases in the upper section of the heater bundle when the blowing upward vapor encounters falling liquid. Then, the first dryout locations move upward as shown in Fig.7, which implies that the flow regime presumably changes from co-current to counter-current at 580kg/m^2s.

3-3. Transition criterion

From the standpoint of the thermal-hydraulic design and safety evaluation of the ATR, the flow condition where dryout power starts to decrease is a prime concern. As discussed in the previous section, this flow condition is presumably closely related to the flow regime transition from co-current downward flow to counter-current flow. It is likely that the transition occurs under the condition in which buoyancy force on the vapor is balanced with drag force generated by falling liquid, and vapor loses its rising or falling speed. On the basis of this

consideration, two models were examined for the evaluation of the transition criterion: the drift flux model and the flooding model. The criterion evaluated by each model was compared with the present experimental results, to find out which model is more adequate for evaluating the transition in the pressure tube housing the ATR fuel bundle.

The drift flux model gives the true velocity of the vapor phase in a two phase mixture. Consequently, the drift flux model predicts that vapor stagnation occurs when the velocity of falling liquid equates the drift velocity, for example, calculated by the following formula derived by Zuber and Findlay[4]:

$$V_{dj} = 1.53(\sigma g/\rho_l)^{1/4} \quad . \qquad (1)$$

Besides this formula, various other formulas for the drift velocity have been proposed, as listed in Table 1.

On the other hand, the flooding model gives an equation correlating the gas and liquid phase specific velocities in counter-current flow. As the correlating equation, the following proposed by Wallis[5] is generally used:

$$J_g^{*1/2} + m J_l^{*1/2} = C \qquad (2)$$

$$J_g^* = J_g \left[\frac{\rho_g}{g D (\rho_l - \rho_g)} \right]^{1/2} \qquad (3)$$

$$J_l^* = J_l \left[\frac{\rho_l}{g D (\rho_l - \rho_g)} \right]^{1/2} \quad . \qquad (4)$$

The flow stagnation of vapor occurs when $J_g^{*1/2} = 0$, that is, when the velocity of liquid phase, $J_l^{*1/2}$ becomes equal to C/m.

Mass velocities corresponding to the void drift velocities for various flow patterns, and to $J_l^{*1/2} = C/m$ are listed in Table 1. In the calculation of the mass velocities in Table 1, The distribution parameter characterizing the drift flux model is assumed to be unity; on the other hand, the empirical constants C

and m in Eq.(2) are chosen to be 0.75 and 1 respectively. These values correspond approximately to those reported by Wallis[5] for a vertical tube. As is seen in Table 1, the mass velocities estimated by the drift flux model are much smaller than the experimental mass velocity of 725kg/m^{2}s at which velocity the flow regime transition is presumed to start, while the mass velocity calculated on the basis of the flooding model agrees well with the experimental value.

Therefore, the flooding model is more favorable than the drift flux model in the evaluation of the transition criterion from co-current downward flow to the counter-current flow inside the ATR fuel bundles.

3-4. Dryout power under the condition of flow stagnation

Under the condition of flow stagnation (mass velocity = 0), the flow regime in the pressure tube seems to be counter-current flow because vapor generated in the pressure tube rises upward due to buoyancy force. It is, therefore, suggested that the dryout power at the flow stagnation condition can be predicted in terms of the flooding model. In order to confirm this suggestion, the dryout power predicted by the flooding model is compared with the present experimental value.

If mass and energy are assumed to balance inside the pressure tube, the following relationship is borne among J_g, J_l and q:

$$J_g \rho_g A = J_l \rho_l A = q A_h / H_{lg} \quad . \quad (5)$$

In counter-current flow, the flow rate of falling liquid is limited by Wallis' flooding equation shown in Eq.(2). The dryout power at the flow stagnant condition is obtained from Eq.(2)-(5) as follows;

$$q = \frac{C^2 A H_{lg} \{\rho_g g (\rho_l - \rho_g) D\}^{1/2}}{A_h \{1 + m^2 (\rho_g / \rho_l)^{1/4}\}^{1/2}} \quad . \quad (6)$$

A flooding CHF model[10] has been employed to estimate dryout power in a thermo-syphone. Mishima[2] applied this model to calculate dryout heat flux under the condition of flow stagnation, and obtained successful results. The equation(6) contains empirical constants,i.e. C and m which depend on geometrical structure and configuration of the test apparatus; however C and m were not determined experimentally for the test apparatus used in the present tests. Thus, by substituting values recently reported for various experimental apparatuses for C and m in Eq.(6), the dryout power for the present test condition was estimated to be 100-220kW. This value has the uncertainty of about 120kW, because the reported values range from 0.75 to 1.1 for C and from 0.9 to 1.1 for m.

The experimental value measured in the present tests is Q=100-350kW. Both agree within the uncertainty. Therefore, the dryout power under the condition of flow stagnation is predictable in terms of the flooding model.

3-5. Pressure drop

Pressure drop is an important factors in the analysis of thermal-hydraulic behavior in a reactor. From this viewpoint, pressure drops were also measured along the 36-rod bundle in the downward flow. The obtained results are shown in Fig.8, and are compared with data measured in upward flow and with calculated values. The calculated values were estimated from pressure loss coefficients which were experimentally determined in the upward flow for each component such as rod bundles and spacers of the 36-rod bundle. As illustrated in Fig.8, the measurements agree well with the calculations over a wide range of mass velocities. In the low mass velocity region, the measured pressure drop is negative. This is attributed to the fact that the static pressure loss has negative value while the accelerational and frictional pressure losses decrease with decreasing mass

velocity. The mass velocity region where the total pressure loss has a negative value coincides with the region where counter-current flow is presumably generated inside the pressure tube.

3-6. Empirical correlation formula for dryout power

Dryout power is important to the prediction of coolability of the downward flow. For convenience in the application to safety analysis codes, an empirical correlation formula was therefore developed from the present experimental data of dryout power, as follows:

(1) $0 \leq G < 458$ kg/m^{2}s , (P=7MPa, Tin=548K)

$$Q\ [MW] = 0.21403 + 1.1243 \times 10^{-3} \times G \qquad (7)$$

(2) $458 \leq G < 725$ kg/m^{2}s , (P=7MPa, Tin=548K)

$$Q\ [MW] = -31.673 + 0.13352 \times G - 1.8354 \times 10^{-4} \times G^2 + 1.1307 \times 10^{-7} \times G^3 - 2.5886 \times 10^{-11} \times G^4 \qquad (8)$$

(3) 725 kg/m^{2}s $\leq G$

In this region, a CHF correlation developed for the upward flow is also available. The CHF correlation is given as a function of several parameters:

$$q = f(X, P, Hsub, Zsp, Dpt, E, LPD, APD) \qquad (9)$$

As seen in Fig.9, it can be concluded from the comparison between predicted and measured data that the present empirical formula can predict the dryout power within an error of $\pm$0.6MW.

4. CONCLUSION

Dryout power in downward flow has been measured on a full scale mock-up of the ATR fuel bundle. It is evident from the experiment that the dryout power in downward flow varies significantly with the flow regime transition. Furthermore, it is demonstrated that a flooding model is available to evaluate the flow regime transition in downward flow.

NOMENCLATURE

A	:Flow cross-sectional area	[m^2]
Ah	:Heater surface area	[m^2]
APD	:Axial power distribution	[-]
C	:Empirical constant	[-]
D	:Hydraulic equivalent diameter	[m]
Dpt	:Pressure tube inner diameter	[m]
E	:Eccentricity in a pressure tube	[m]
G	:Mass flux	[kg/m^2s]
g	:Acceleration by gravity	[m/s^2]
H	:Enthalpy	[J/kg]
J	:Superficial flow velocity	[m/s]
J^*	:Non-dimensional flow velocity	[-]
LPD	:Local power distribution	[-]
m	:Empirical constant	[-]
P	:Pressure	[Pa]
q	:Heat flux	[kW/m^2]
Q	:Input power	[MW]
T	:Temperature	[K]
Vdj	:Drift velocity	[m/s]
X	:Steam quality	[-]
Zsp	:Spacer pitch	[m]
	:Surface tension	[N/m]
	:Density	[kg/m^3]

Subscripts:

g	:Gas phase
l	:Liquid phase
lg	:l - g
sub	:Subcooling

REFERENCE

[1] M.Cumo, et al., Up-Flow and Down-Flow Burnout, Conf. Heat Fluid Flow Water Reactor Saf., (GBR), p.183-192,(1977)
[2] K.Mishima, et al., The Effect of Flow Direction and Magnitude on CHF, Nuclear Engineering and Design, 86, p.165-181 (1985)
[3] J.G.Collier, Future Research Suggestions on Boiling and Condensation, Advances in Two-phase Flow and Heat Transfer, Vol.2,p.877-895 (1983)
[4] Zuber,N. et al. 3rd. Int. Heat Transfer Conf.,5,p.24-38(1966)
[5] G.B.Wallis, One-dimensinal Two-phase Flow, McGraw-Hill,(1969)
[6] Peebles,F.N. et al. Chemical Engineering Prog. 49, p.88(1953)
[7] Nicklin,D.J. et al. Trans.Inst.Chemical Engineering. 40(1962)
[8] Zuber,N.,and Findlay, Trans. ASME J. Heat Transfer 87 ser.C, p.458 (1965)
[9] Ishii,M., Thermo-fluid Dynamic Theory of Two-Phase Flow, Eyrolles, Paris (1975)
[10] Y.Katto, Critical Heat flux, Advances in Heat Transfer, vol.17, Academic Press Inc.

Table 4-1 Drift Velocity Comparison

NAME	FLOW PATTERN	DRIFT VELOCITY EQUATION	DRIFT VELOCITY [m/sec]	CORRESPONDING MASS VELOCITY[Kg/m^2·sec]
Zuber	LARGE-BUBBLE	$V_{dj} = 1.18 \left[\frac{\sigma(\rho_l - \rho_g)g}{\rho_l^2} \right]^{1/4}$	0.144	106.5
Shulman	LARGE-BUBBLE	$V_{dj} = 0.35 \left[\frac{D(\rho_l - \rho_g)g}{\rho_l} \right]^{1/2}$	0.103	76.22
Nicklin	SLUG FLOW	$V_{dj} = 0.35 \ (gD)^{1/2}$	0.106	78.40
Zuber & Findlay	CHURN-TURBULENT	$V_{dj} = 1.53 \ (\sigma g / \rho_l)^{1/4}$	0.107	79.20
Ishii	CHURN-TURBULENT	$V_{dj} = 1.41 \left[\frac{\sigma(\rho_l - \rho_g)g}{\rho_l^2} \right]^{1/4}$	0.097	71.80

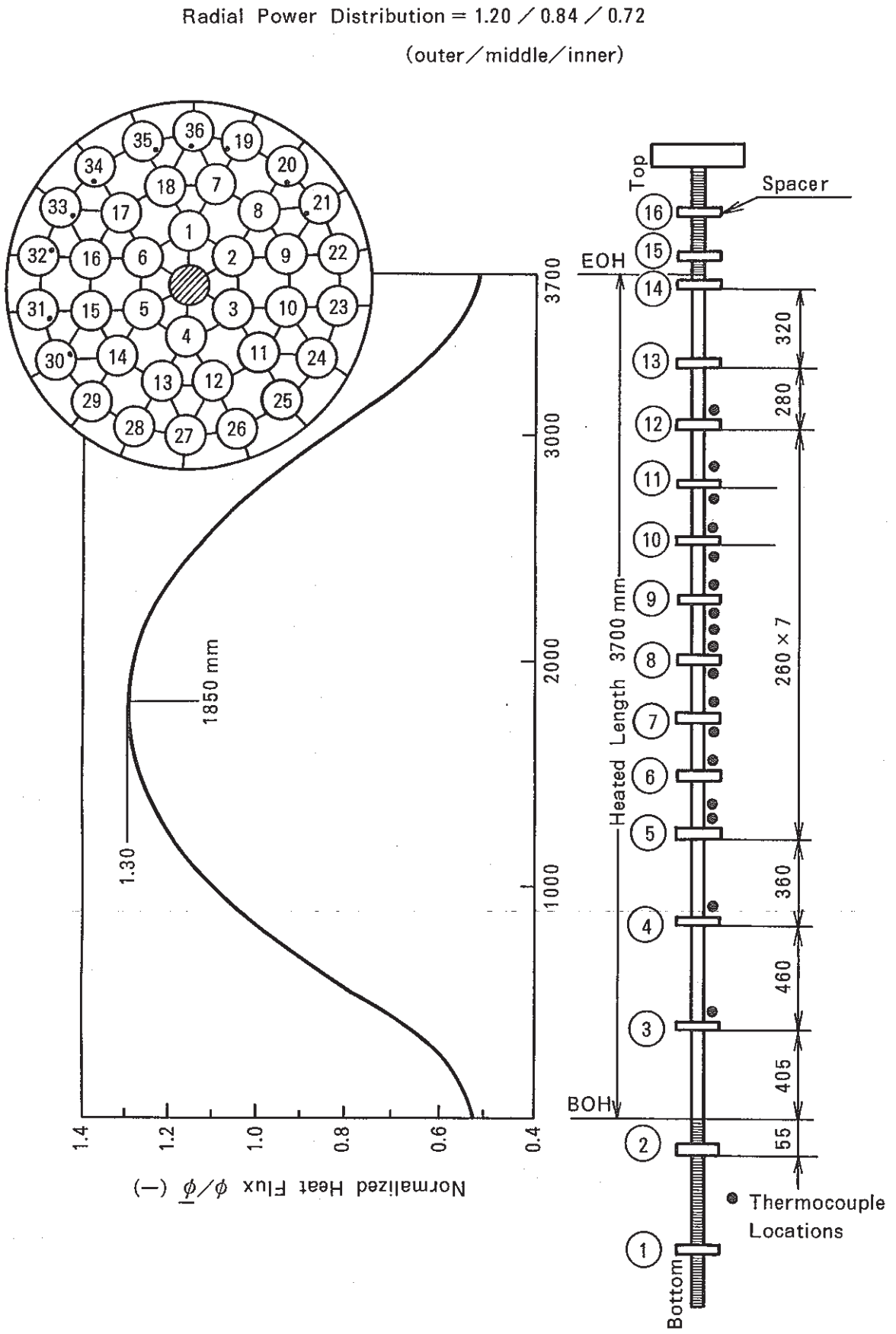

Fig. 1 Examples of Axial Power Distribution and Thermocouple Locations For Downward Flow (Spacer Locations are same as 600 MWe Demonstration ATR)

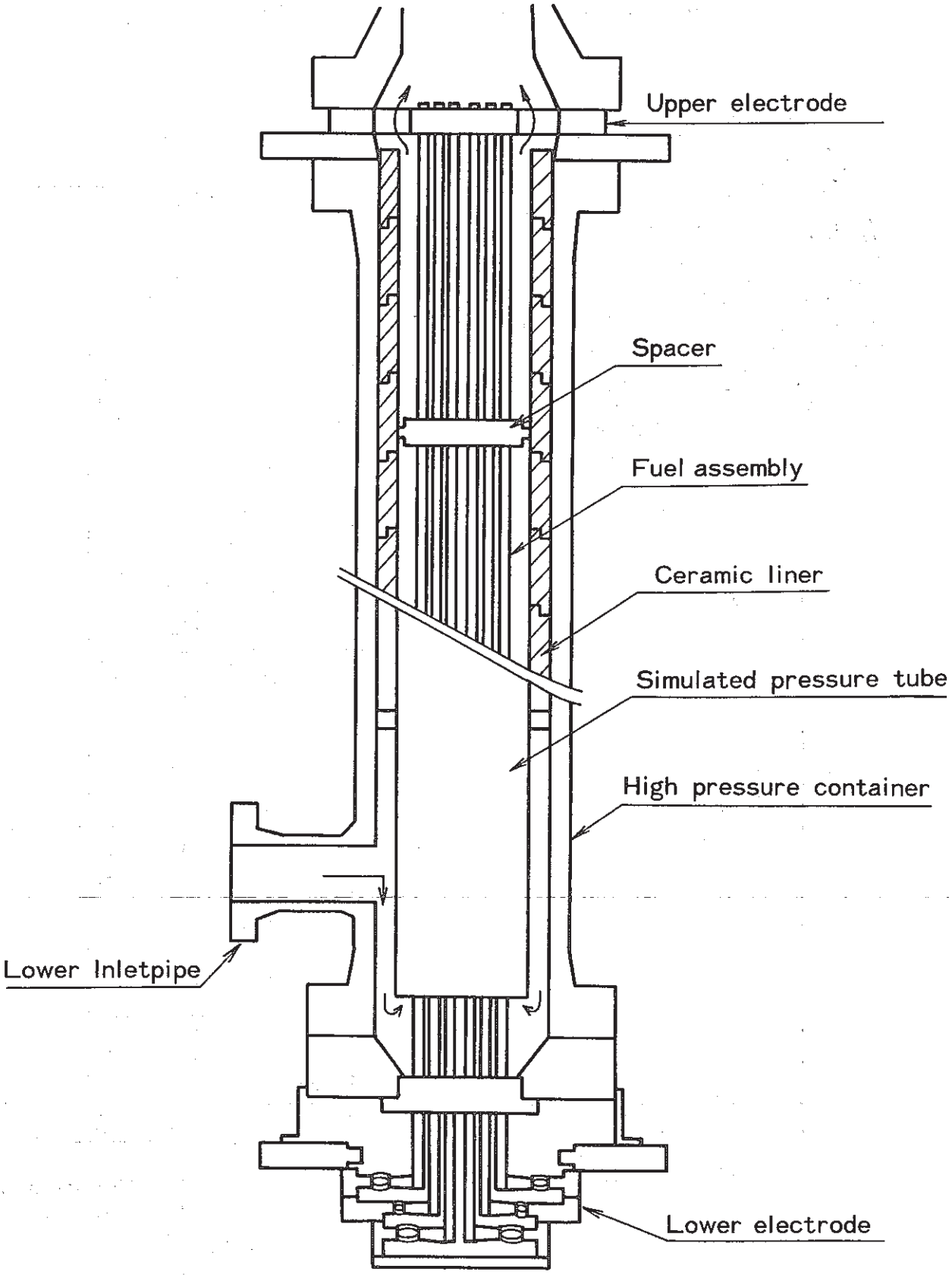

Fig. 2 Test Section

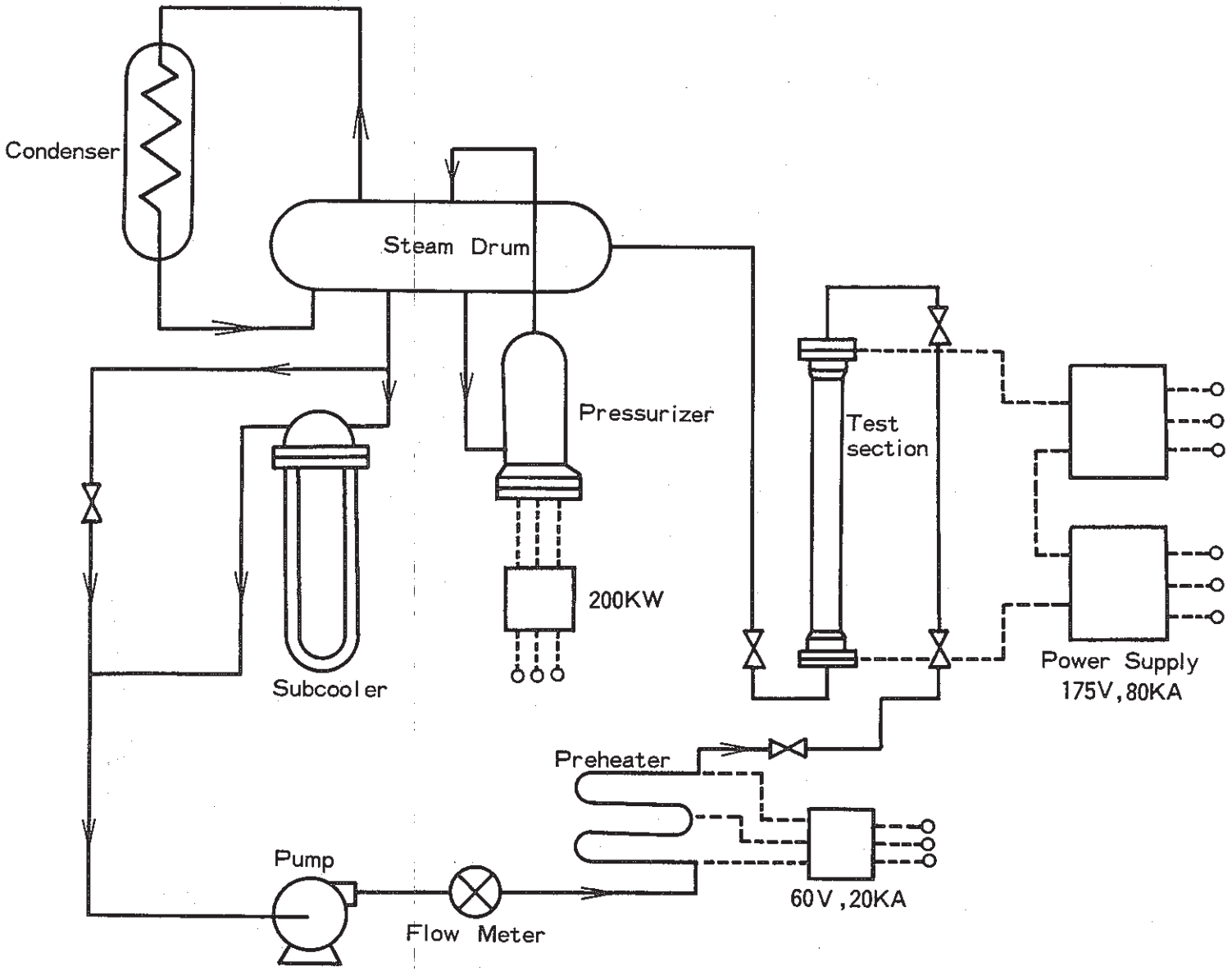

Fig.3 Flow Diagram of the 14MW Heat Transfer Loop (HTL)

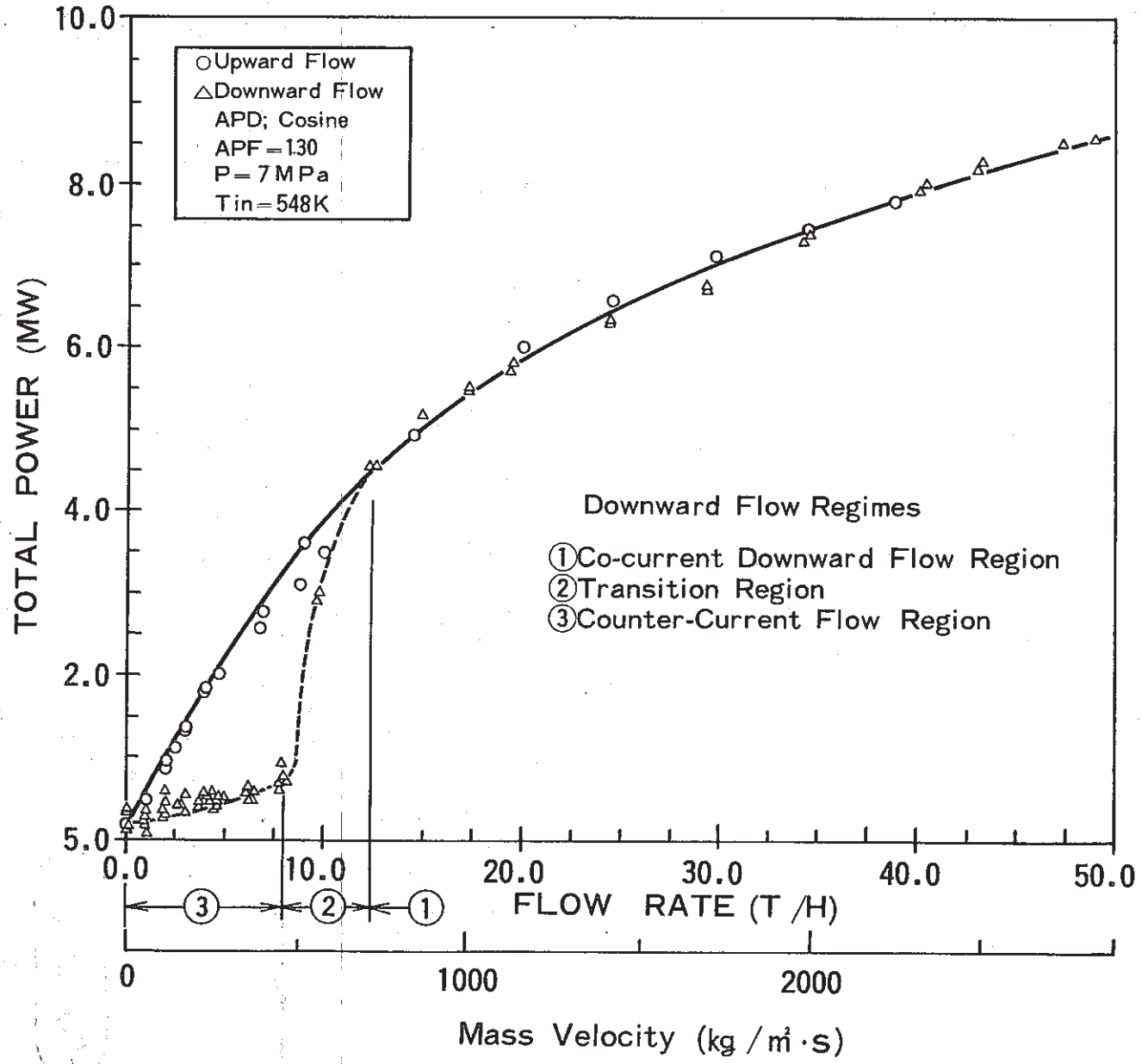

Fig. 4 Experimental Results of Dryout Power

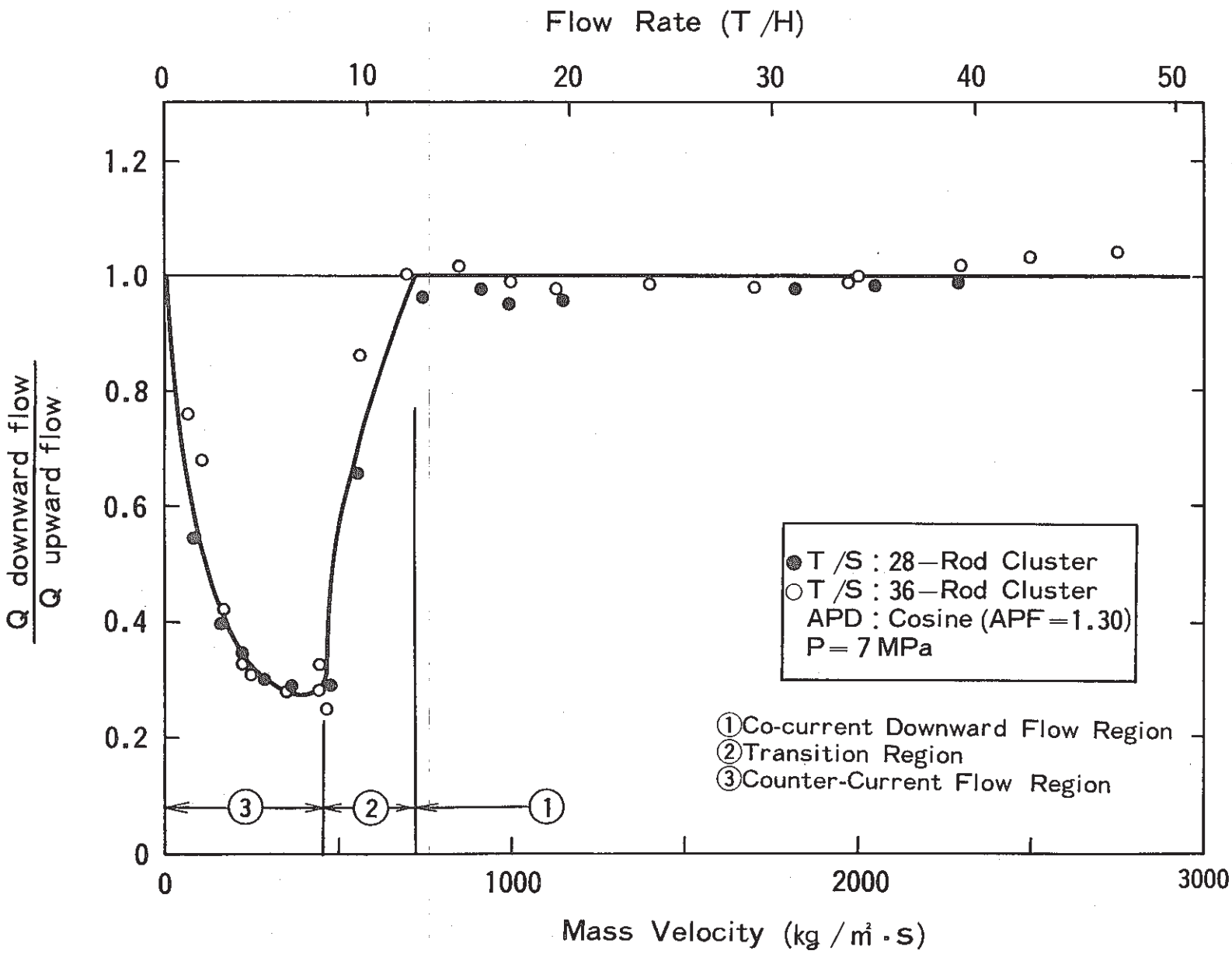

Fig. 5 Effect of Downward Flow on Dryout Power

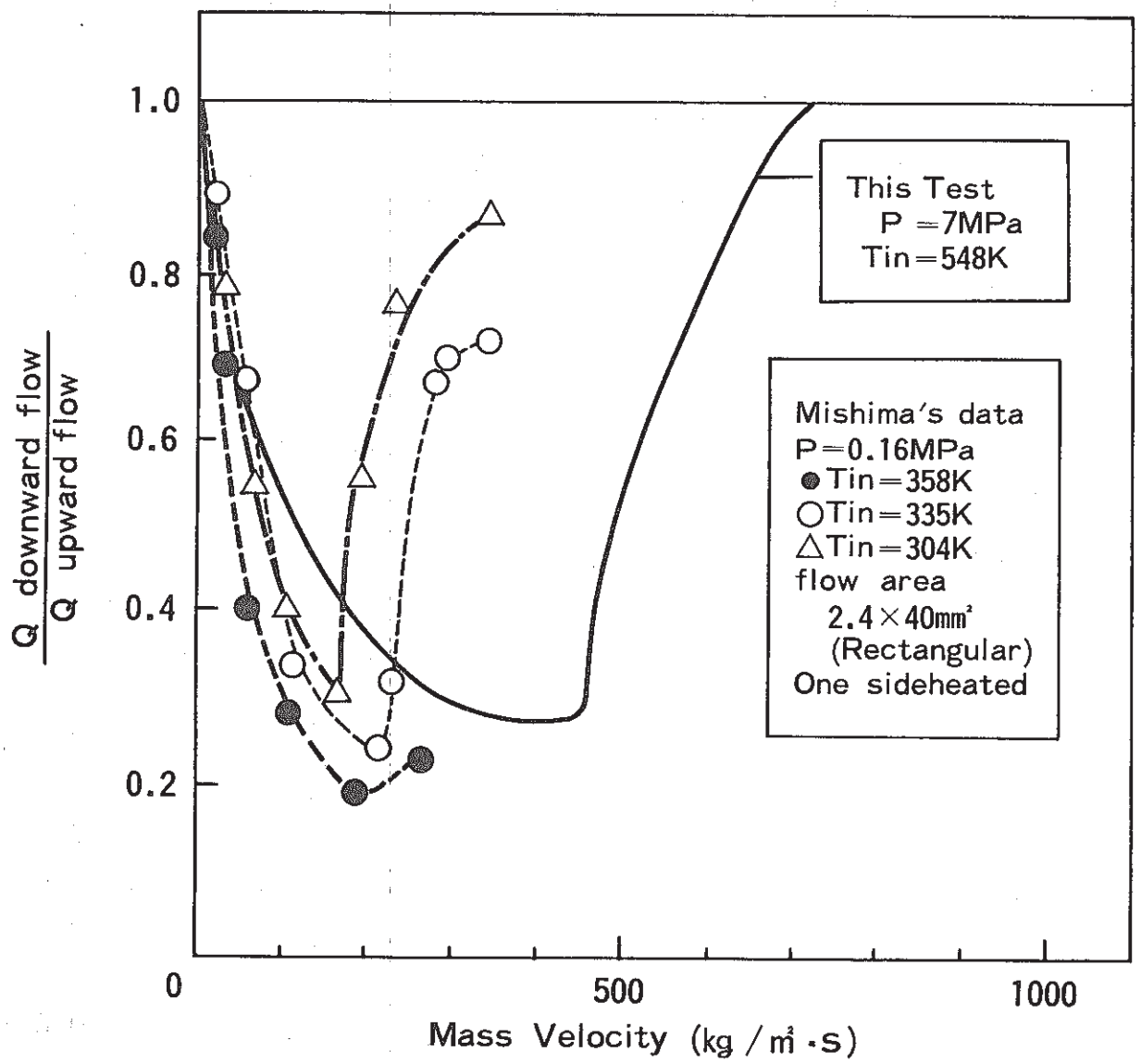

Fig. 6 Comparison with Mishima's data

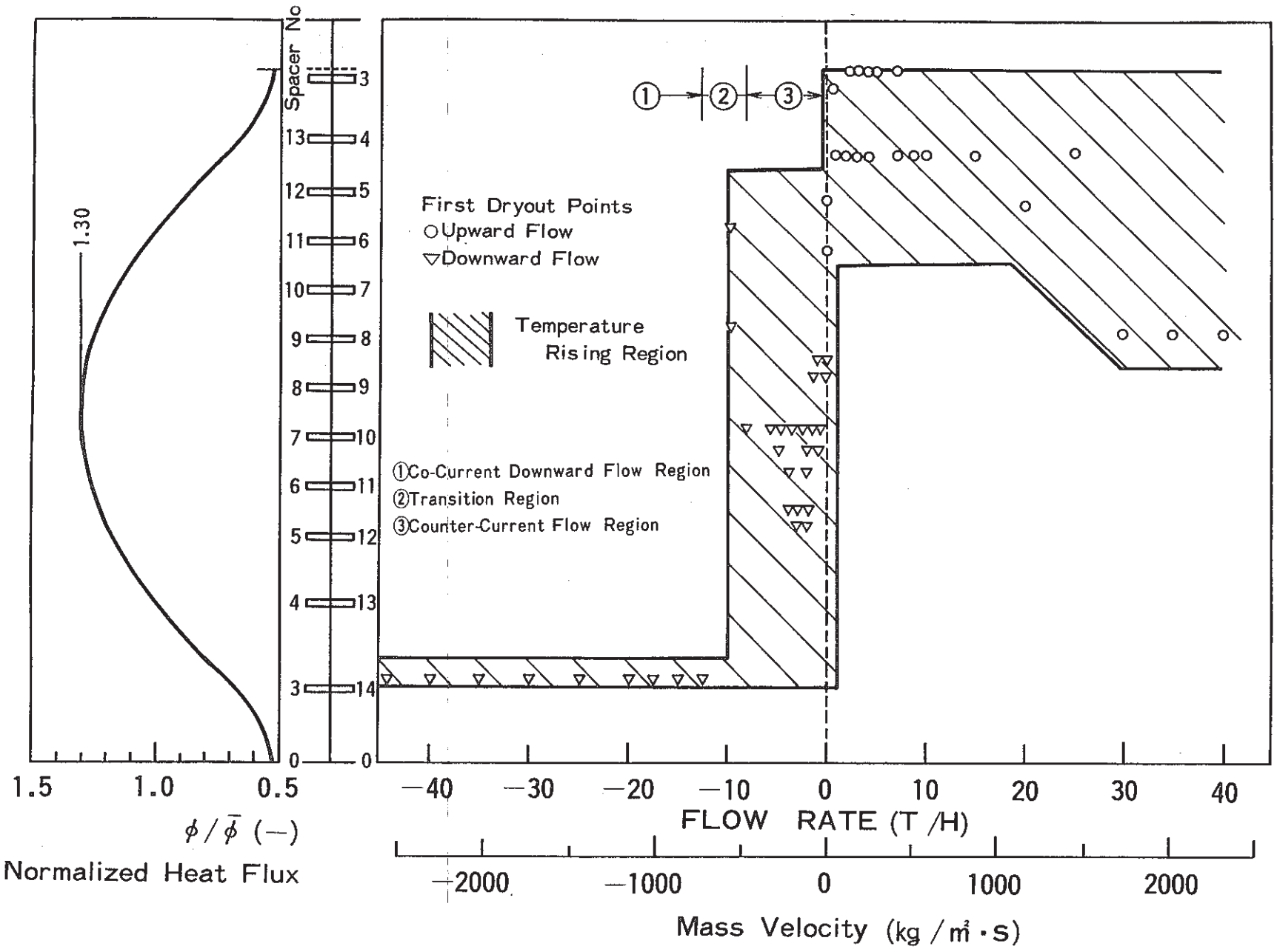

Fig. 7 Axial Location of Dryout Points

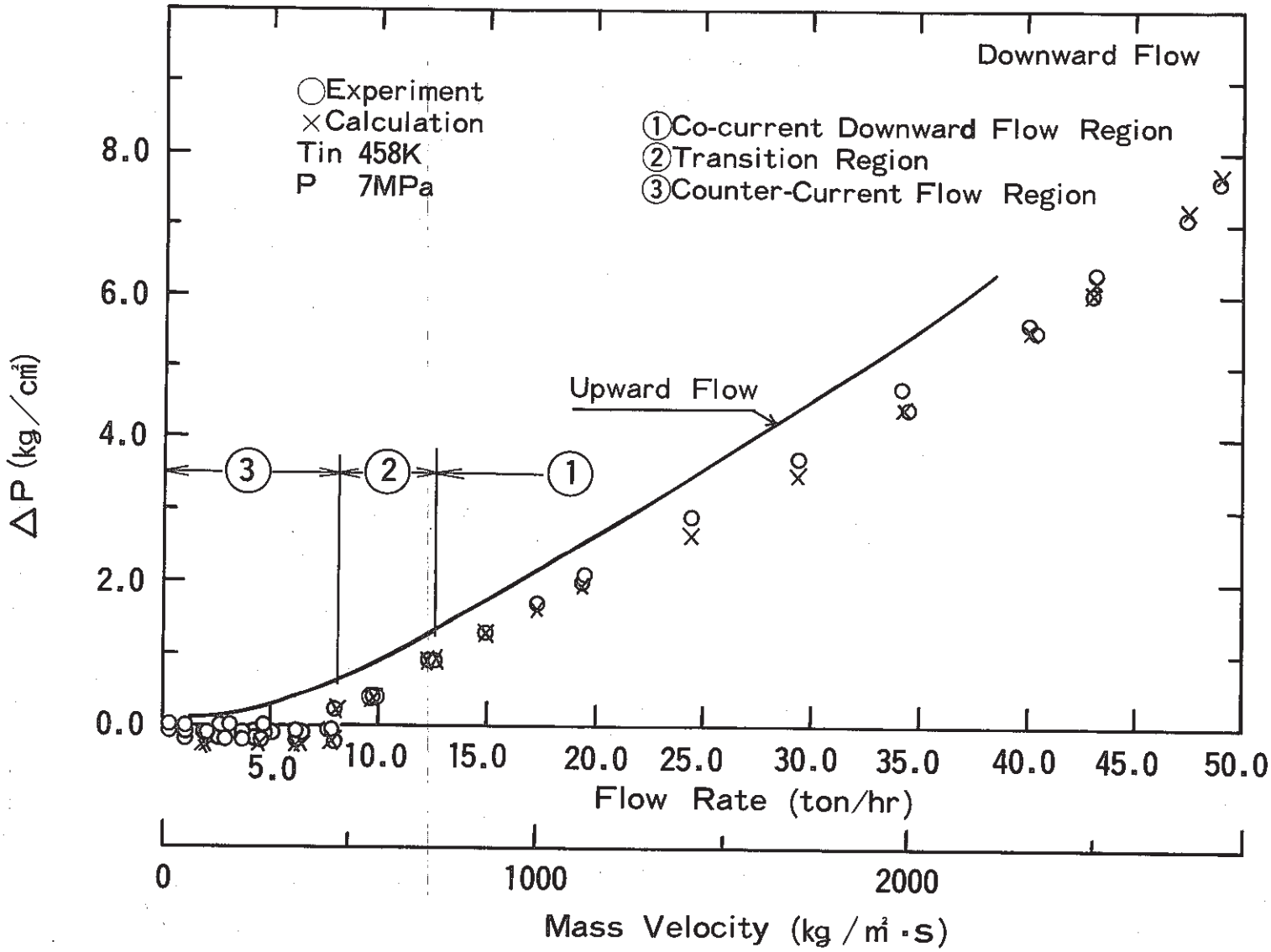

Fig.8 Comparison of Differential Pressure between Calculation and Experiment in Downward Flow

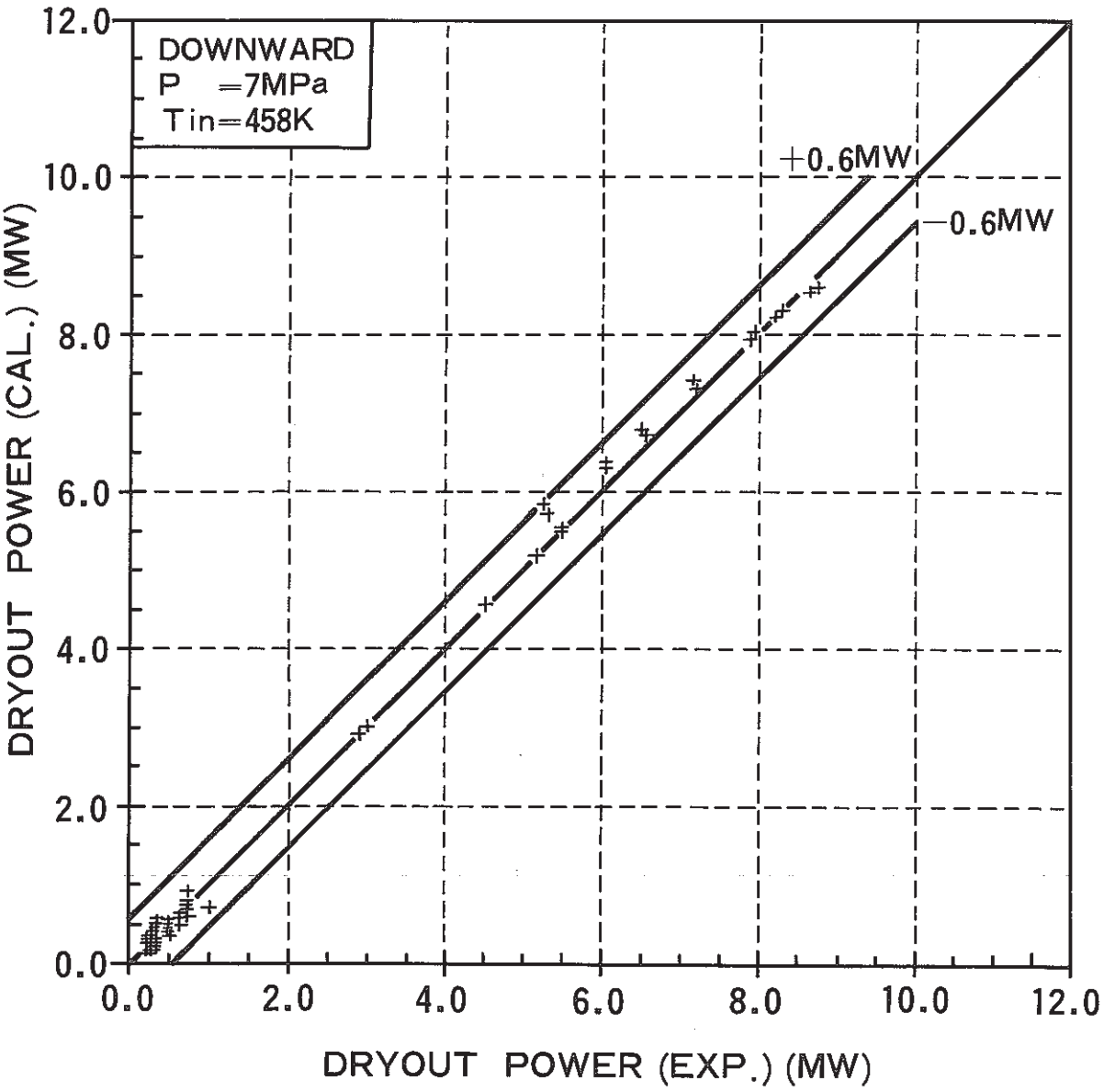

Fig.9 SCATGRAM OF DRYOUT POWER
(Downward Flow)